Behavioral/Systems/Cognitive

Encoding of Movement Direction in Different Frequency Ranges of Motor Cortical Local Field Potentials

Jörn Rickert,[1,2]* Simone Cardoso de Oliveira,[2] Eilon Vaadia,[4] Ad Aertsen,[1,2] Stefan Rotter,[1,2,5] and Carsten Mehring[2,3]*

[1]Department of Neurobiology and Biophysics, Institute of Biology III, [2]Bernstein Center for Computational Neuroscience, Center for Neural Dynamics Freiburg, and [3]Department of Neurobiology and Animal Physiology, Institute of Biology I, Albert-Ludwigs-University, 79104 Freiburg, Germany, [4]Department of Physiology, Hadassah Medical School, and Interdisciplinary Center for Neural Computation, The Hebrew University of Jerusalem, Jerusalem 91120, Israel, and [5]Theory and Data Analysis, Institute for Frontier Areas of Psychology and Mental Health, 79098 Freiburg, Germany

Recent studies showed that the low-frequency component of local field potentials (LFPs) in monkey motor cortex carries information about parameters of voluntary arm movements. Here, we studied how different signal components of the LFP in the time and frequency domains are modulated during center-out arm movements. Analysis of LFPs in the time domain showed that the amplitude of a slow complex waveform beginning shortly before the onset of arm movement is modulated with the direction of the movement. Examining LFPs in the frequency domain, we found that direction-dependent modulations occur in three frequency ranges, which typically increased their amplitudes before and during movement execution: ≤4, 6–13, and 63–200 Hz. Cosine-like tuning was prominent in all signal components analyzed. In contrast, activity in a frequency band ≈30 Hz was not modulated with the direction of movement and typically decreased its amplitude during the task. This suggests that high-frequency oscillations have to be divided into at least two functionally different regimes: one ≈30 Hz and one >60 Hz. Furthermore, using multiple LFPs, we could show that LFP amplitude spectra can be used to decode movement direction, with the best performance achieved by the combination of different frequency ranges. These results suggest that using the different frequency components in the LFP is useful in improving inference of movement parameters from local field potentials.

Key words: **motor cortex; local field potential; brain-machine interface; voluntary movement; neural coding; oscillations**

Introduction

Recent technological breakthroughs in neuroscience have demonstrated the feasibility of using brain activity directly as a control signal for an external actuator, like a prosthetic device (Serruya et al., 2002; Taylor et al., 2002; Carmena et al., 2003). In this context, it is important to examine the neuronal signals that can optimally serve this purpose (Andersen et al., 2004). The most easily accessible signal is the electroencephalogram (EEG), recorded noninvasively (Wolpaw et al., 2002; Wolpaw and McFarland, 2004). However, this signal is limited in its spatial resolution. At the other end of the methodological spectrum lies the spiking activity of single neurons (SUA), providing highest spatial and temporal resolution but being most invasive and most difficult to obtain and maintain for long periods. For a resolution between these two extremes, recent studies have shown that local field potentials (LFPs), recorded by intracortical microelectrodes like SUA (Pesaran et al., 2002; Mehring et al., 2003) and electrocorticograms (ECoGs), recorded subdurally from the surface of the brain (Leuthardt et al., 2004; Mehring et al., 2005), can serve as an alternative signal for decoding movement direction. LFPs and ECoGs, which predominantly reflect the synaptic activities of more or less local populations of neurons (Mitzdorf, 1985), are presumably more stable than SUA, both against mechanical perturbations and during long-term recordings. Moreover, LFPs/ECoGs can be easily obtained from the raw electrode signal by low-pass filtering, in contrast to the complex procedure of spike sorting required for SUA. Thus, intracranial population signals such as the LFP and the ECoG should be especially useful for neural prosthetic applications. Compared with SUA, the knowledge about how information is encoded in these signals is still limited.

Here, we examined features of motor cortical LFPs in the temporal and the frequency domain, complementary to our previous study (Mehring et al., 2003) in which only the low-frequency component of the signal was analyzed in the time domain. We found information on the direction of arm movements in the movement-evoked potential (mEP) in the time domain and, additionally, in the amplitudes of distinct low- and high-frequency bands of the LFP (≤4, 6–13, and 63–200 Hz).

Materials and Methods

Experimental procedures. Two female rhesus monkeys (*Macaca mulatta*; monkey P and monkey G) were trained to operate two separate low-weight, low-friction manipulanda, one with each arm. The manipulanda

Received March 1, 2005; revised Aug. 3, 2005; accepted Aug. 4, 2005.

This work was supported in part by the German Federal Ministry of Education and Research [Bundesministerium für Bildung und Forschung (BMBF)–Deutsche–Israelische Projektkooperation and BMBF Grant 01GQ0420], the German-Israeli Foundation for Scientific Research and Development, the United States–Israel Binational Science Foundation, the Israeli Science Foundation, and the WIN-Kolleg of the Heidelberg Academy of Sciences and Humanities. We thank Anna Gribova for her contribution to the experimental work.

*J.R. and C.M. contributed equally to this work.

Correspondence should be addressed to Jörn Rickert, Neurobiology and Biophysics, Institute of Biology III, Albert-Ludwigs-University, Schänzlestraße 1, 79104 Freiburg, Germany. E-mail: rickert@biologie.uni-freiburg.de.

DOI:10.1523/JNEUROSCI.0816-05.2005

 0270-6474/05/258815-10$15.00/0

were freely moveable in the horizontal plane and controlled the motion of two cursors on a vertically oriented video screen placed in front of the monkey. The monkeys were trained to perform unimanual center-out movements with either arm in response to a visual cue. All movements started from central resting positions located in front of each shoulder and ended in one of eight targets that were regularly arranged on a circle with a 3 cm radius around the respective resting position.

In each monkey, two recording chambers (27 × 27 mm) were surgically implanted above the left and the right hemispheres while the monkeys were under general anesthesia. Animal care and surgery procedures were in accordance with the National Institutes of Health *Guide for the Care and Use of Laboratory Animals* and the Hebrew University regulations. Neural activity was recorded with eight glass-coated tungsten microelectrodes (impedance, 0.2–0.8 MΩ at 1 kHz) from homologous sites in the two hemispheres (four electrodes in each hemisphere, interelectrode distances between 350 and 700 μm).

Data acquisition and preprocessing. The raw neural signal recorded on each electrode was filtered (multichannel processor; Alpha-Omega, Nazareth, Israel) with a bandpass of 1–150 Hz to extract the LFP and filtered with a bandpass of 300–8000 Hz to obtain the action potentials. The spikes were sorted on-line (multispike detector; Alpha-Omega) to detect and isolate single-unit activity. Multiunit activity (MUA) was then generated by merging all isolated spike trains recorded from one electrode. The low-pass component of the hardware filter used to extract the LFP had a transfer characteristic of $V_{out}/V_{in} = 1/\sqrt{1+(f/fc)^4}$, where fc is the cutoff frequency (here, 150 Hz). Thus, the amplitudes at 150 and 200 Hz were reduced by a factor of ≈1.4 and ≈2.0, respectively. Electrode recordings that yielded entirely flat LFPs (approximately one-fifth of the complete number of recording sites) were excluded, and measurements from 210 different recording sites, resulting in 419 LFPs for ipsilateral and contralateral movements, were analyzed. All data were sampled at 400 Hz. For analysis of LFPs in the time domain, the data were filtered with a 50 Hz notch filter to reduce noise artifacts at 50 Hz, most likely induced by the electrical power system.

Time-resolved LFP amplitude spectra. Time-resolved LFP amplitude spectra between 750 ms before and 1000 ms after movement onset were calculated for each trial individually by a short-time discrete Fourier transform (DFT) (Press et al., 1992) using a sliding Hamming window of 145 bin (362.5 ms) width. Before applying the DFT, we zero-padded the signals in the time domain to obtain an exact band-limited interpolation of the spectra in the frequency domain (Smith, 2003) at a resolution of 1 Hz.

To dissect amplitude changes for different frequencies during the time course of the trial, we computed normalized amplitude spectra in the following way: for each frequency bin, we divided the time-resolved amplitude by the baseline amplitude for this frequency. The latter was determined as the mean amplitude of the frequency in the time interval between 750 and 375 ms before the presentation of the visual cue, averaged across trials (i.e., all trials of the corresponding LFP electrode). For the grand mean spectrum of Figure 4*b*, the baseline amplitude was additionally averaged across all LFP recordings.

To verify whether the amplitude of a frequency band increased (decreased) during movement, we tested whether the trial-averaged normalized amplitude in that band during movement was above (below) 1 with a 95% confidence interval estimated from the SEM (i.e., under the assumption of a Gaussian distribution for the single trials around the mean).

We investigated the LFP amplitude spectra with frequencies up to 200 Hz. Because higher frequencies are potentially contaminated with residual spiking activity, one might argue that this frequency range could be just a reflection of filtered spiking activity from nearby neurons. However, two findings argue against this hypothesis. First, the observed changes in relative amplitude were very similar over the entire frequency range of 63–200 Hz. Although a residue of spiking activity at 200 Hz in the low-pass-filtered signal might be possible (typical cutoff frequencies for the high-pass filter applied before spike sorting are in the range of 150–500 Hz; in our study, 300 Hz), the presence of such spike residue at frequencies as low as 63 Hz is very unlikely. Second, the noise correlation (i.e., the correlation between trial-by-trial fluctuations) in the 63–200 Hz band of LFPs and simultaneously recorded MUA from the same electrode was very low (≈0.1; data not shown) before, during, and after the movement.

Analysis of directional tuning. We analyzed the directional tuning of the movement-evoked LFP in the time domain and of the amplitudes of the LFP components in different frequency bands. Tuning curves were determined by computing the trial-averaged signals (amplitude or movement-evoked potential) as a function of movement direction. We characterized the tuning curves by two different measures: (1) the tuning strength and (2) for significantly tuned signals, the similarity of the tuning curve to a cosine function.

As a measure of tuning strength, we computed the signal-to-noise ratio (SNR) of the tuning curve by the following equation:

$$\mathrm{SNR} = \frac{\sigma_s^2 - \sigma_b^2}{\sigma_n^2}.$$

Here, σ_s^2 is the variance of the tuning curve, σ_n^2 is the variance of the trial-by-trial fluctuations, and σ_b^2 is the variance of the tuning curve that is induced in the presence of noise if only a limited number of trials are measured for each direction. Under the assumption of a Gaussian noise distribution an estimate for this term is as follows:

$$\sigma_b^2 = \frac{1}{8N}\sum_{tr=1}^{s}\sigma_{tr}^2,$$

where σ_{tr}^2 is the variance of the trial-by-trial fluctuations for each specific target tr and N is the number of trials for each target. To compute the significance level (p value) of the tuning, we compared the SNR value to the chance distribution for a flat tuning curve. The chance distribution was obtained numerically by computing 500 times the SNR of the same signals with a random relationship between signals and directions.

For significantly ($p < 0.05$; see above) tuned signals, we investigated whether the directional modulation was cosine like. To this end, we fitted a cosine function [$y = a + b \times \cos(x) + c \times \sin(x) = a + d \times \cos(x - \varphi)$, where φ is the preferred direction (PD)] to the trial-averaged signal by a weighted least-squares fit using the inverse of the squared SEMs as weights. To assess the degree of cosine tuning, we computed the squared correlation coefficient (r^2) between the fit and the trial-averaged signal and compared the distribution of r^2 inferred from our data with the distribution of r^2 inferred from a population of 10,000 randomly generated tuning curves; each curve consisted of eight random values from the interval [0, 1]. The significance of the deviation between the two distributions was verified by the Wilcoxon rank sum test.

Signal and noise correlation. We computed the signal and noise correlations between different frequency bands of LFPs. The signal correlation r_s measures the similarity of the directional tuning of two frequency bands of the same LFP. The signal correlation was calculated as the correlation coefficient between tuning curves (i.e., between the average activities of the eight directions) as follows:

$$r_s = \frac{\frac{1}{8}\sum_{i=1}^{8}\left(\left(v_i - \frac{1}{8}\sum_{j=1}^{8} v_j\right)\left(w_i - \frac{1}{8}\sum_{j=1}^{8} w_j\right)\right)}{\sigma_v \sigma_w},$$

where v_i and w_i are the trial-averaged amplitudes of the two frequency bands for direction i and σ_v and σ_w are the SDs of v_i and w_i.

The noise correlation r_n measures the correlation between the trial-by-trial fluctuations of the amplitudes of two frequency bands of the same LFP. The noise correlation was calculated as follows:

$$r_n = \left\langle \frac{\frac{1}{N_i}\sum_{j=1}^{N_i}(x_i^j - v_i)(y_i^j - w_i)}{\sigma_{xi}\sigma_{yi}} \right\rangle_{i=1..8},$$

where x_i^j and y_i^j are the single-trial amplitudes of the two frequency bands for direction i and trial j, σ_{xi} and σ_{yi} are their SDs for direction i, and N_i is the number of trials for direction i.

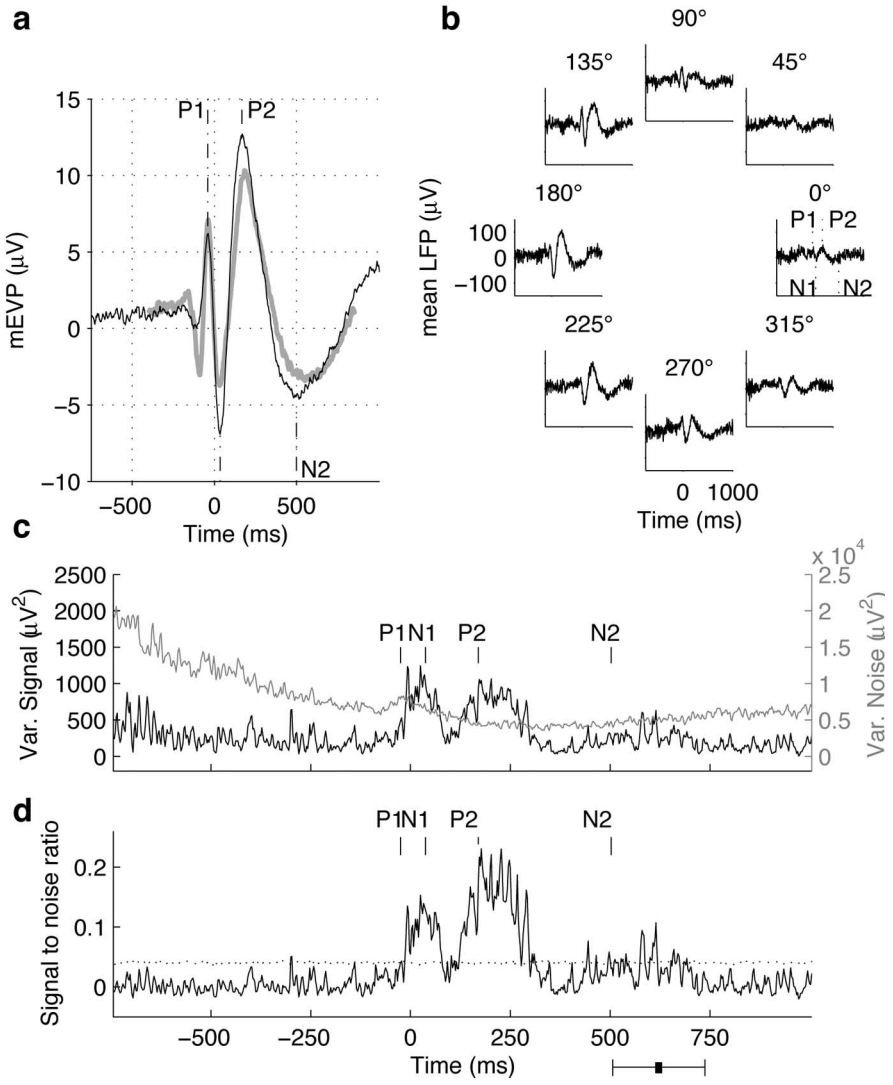

Figure 1. Tuning of the movement-evoked potential. Time 0 ms indicates movement onset. ***a***, Grand average mEP (averaged across all recorded LFPs). Trials were aligned either to movement onset (black curve) or to cue onset (gray curve). P1, P2, N1, and N2 indicate the points in time of the positive and negative peaks of the average LFP. ***b***, Directional tuning of an mEP obtained from a single electrode: trial-averaged activity shown separately for each movement direction. ***c***, Time-resolved strength of the directional modulation (signal, black curve, left vertical axis) and variance (Var.) of the trial-by-trial fluctuations (noise, gray curve, right vertical axis) for the mEPs shown in ***b***. ***d***, Time-resolved signal-to-noise ratio of the mEP tuning shown in ***b***. The dotted line indicates threshold for significant tuning ($p < 0.05$; see Materials and Methods). The black bar below the plot shows the average time of movement end and its SD for this recording session.

Single-trial decoding of LFPs. LFP signals were decoded on a single-trial basis by regularized linear discriminant analysis (Friedman, 1989). To calculate the probability of correct decoding [termed decoding power (DP)], we used 15 randomly drawn test trials for each movement direction and computed the DP as the number of trials with correct classifications divided by the total number of 120 test trials. This procedure was repeated 50 times (for single- and eight-channel decoding) or 10 times (for 48-channel decoding), and the average decoding power was taken. Trials used to train the discriminant were not included in the test set for decoding. For the decoding analysis, we used only data from the experimental sessions with eight simultaneous LFP recordings. This subset contained recordings from 17 recording sessions and 80 different electrode sites. As inputs to the classifier, we used either the LFP in the time domain or the amplitudes of the LFP in different frequency bands, as described below.

Decoding the LFP in the time domain. Decoding of the LFP in the time domain was done by the following two procedures after low-pass filtering the signals by a third-order Butterworth filter with 13 Hz cutoff frequency. (1) For each LFP, a D-dimensional vector was constructed from the smoothed LFPs between 200 ms before movement onset and movement end, resampled at 26.7 Hz. For a given set of N LFPs, these D-dimensional vectors were concatenated yielding an $N \times$ D-dimensional signal vector for each trial. These signal vectors were then used as inputs to the linear discriminant. (2) To determine how well the tuning of LFPs in the time domain can be described by a modulation of the amplitude of a direction invariant waveform, the time course of the smoothed LFP in trial i was modeled as $\mathrm{LFP}_i(t) = a_i \times \mathrm{mEP}(t) + c_i$, where $\mathrm{mEP}(t)$ is the movement-evoked potential (i.e., the smoothed LFP response averaged across all trials and directions) and a_i and c_i are the amplitude and offset in trial i obtained by a least-squares fit of $\mathrm{LFP}_i(t)$ to $\mathrm{mEP}(t)$. The scalars a_i were then used as inputs to the classifier.

Decoding the LFP in the time-frequency domain. We decoded the temporal evolution of the amplitudes of three different frequency bands (≤4, 6–13, and 63–200 Hz) and their various combinations. To this end, for each LFP and each frequency band, an M-dimensional vector was constructed by using the time-resolved normalized amplitudes between 200 ms before movement initiation and movement end, resampled at 25 Hz. For a given set of eight simultaneously recorded LFPs, these M-dimensional vectors were concatenated yielding an $8 \times$ M-dimensional signal vector for each trial and for each frequency band. These signal vectors were then used as inputs to the linear discriminant. Different frequency bands were decoded by separate discriminants. Alternatively, we applied the discriminant to the concatenation of signal vectors from multiple frequency bands and found that this yielded lower decoding powers (data not shown). To estimate the decoding power for 48 LFP channels, signal vectors recorded in separate sessions with eight channels per session were decoded by separate discriminants. The decoding power of $N = 100$ different combinations of 6 of 17 recording sessions was computed.

Results

LFP tuning in the time domain

As demonstrated in previous studies (Donchin et al., 2001), averaging LFPs across trials and directions with alignment to movement onset yields a slow complex waveform, the mEP. The mEP typically exhibits two positive (P1, P2) and two negative (N1, N2) peaks (Fig. 1*a*) uniformly across electrodes and with little variation in peak position. With trials aligned to the visual cue signal, two additional peaks, one positive and one negative, precede P1 (Fig. 1*a*, gray curve). For the majority of LFPs (67%), the mEP and also the tuning (see below) was larger with alignment to movement onset. Therefore, all additional results presented in this paper are shown for LFPs aligned to movement onset. Nonetheless, all results presented here were qualitatively reproducible with alignment to cue onset.

Figure 1*b* illustrates the directional tuning of a sample mEP recorded by a single electrode during execution of contralateral movements. Note that this mEP is strongly tuned, with the high-

est amplitude for movement to the left (180°). To further explore the directional modulation of this mEP, we determined the time-resolved SNR of the mEP tuning (see Materials and Methods). Figure 1*c* shows the temporal evolution of the magnitude of the directional modulation (signal; black curve) and the magnitude of the trial-by-trial fluctuations (noise; gray curve) for this mEP. Between the time of movement onset and ≈300 ms after movement onset, the signal strength increased substantially and exhibited two clear peaks. The noise started to decrease >500 ms before movement initiation and was reduced during movement execution. The SNR (Fig. 1*d*) showed a significant increase around the times of N1, P2, and N2 ($p < 0.05$; see Materials and Methods), resulting from both a reduction of the trial-by-trial fluctuations and an increase in the direction-dependent modulation. Between the peaks, the SNR decreased again to ≈0. Note, that the signal was not smoothed here to keep temporal fluctuations, although the maximum of the SNR could be increased by smoothing.

Next, we examined the tuning curves of this sample mEP at the times of the four peaks: P1, N1, P2, and N2. Significant directional tuning ($p < 0.05$; see Materials and Methods) was present at N1, P2, and N2. The tuning around N1, P2, and N2 fitted cosine functions well ($r^2 = 0.74$, 0.85, and 0.95 for N1, P2, and N2, respectively), as shown in Figure 2*a*.

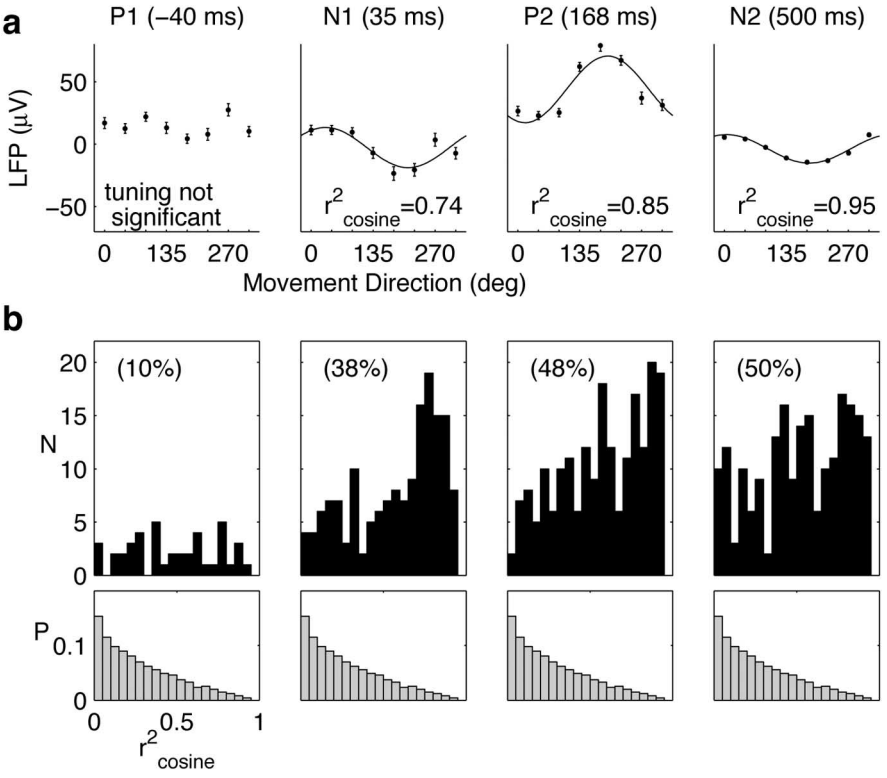

Figure 2. Cosine tuning of mEPs in the time domain. Correlations with cosine tuning curves are depicted separately for each peak (P1, N1, P2, and N2 from left to right). Data were smoothed with a Gaussian kernel of standard width of 50 ms (analysis for P1, N1, and P2) or 125 ms (analysis for N2). ***a***, Dependence on movement direction of mean activity (black dots) and SEM (small black bars) of the sample mEPs shown in Figure 1*b*. For the peaks with significant tuning ($p < 0.05$; see Materials and Methods), a cosine curve was fitted to the data (black curves; see Materials and Methods for details). The time indicated above each panel is the time relative to movement onset. The number below each curve is the squared correlation coefficient r^2_{cosine} between data and the fitted cosine function. ***b***, Correlation between mEP tuning curves and fitted cosine function for all mEPs with significant tuning ($p < 0.05$; see Materials and Methods). The percentage of these mEPs from the total number of mEPs recorded is given in parentheses. The top panels show the distribution of values for r^2 at P1, N1, P2, and N2, respectively. Gray histograms (bottom) depict the distribution of r^2 values obtained for random tuning curves (see Materials and Methods).

The behavior of this sample mEP was indeed typical for many motor cortical LFPs, as revealed by the population analysis of all recorded LFPs (Fig. 2*b*). We found that 16% of all mEPs were significantly ($p < 0.05$; see Materials and Methods) tuned during P1, 38% during N1, 48% during P2, and 50% during N2. Figure 2*b* shows that the tuning curves of these mEPs fitted cosine functions well: r^2 at N1 was higher than 0.7 in 47%, r^2 at P2 was higher than 0.7 in 40%, and r^2 at N2 was higher than 0.7 in 36% of the significantly tuned mEPs. For all peaks, the distribution of r^2 values differed significantly from the distribution of r^2 obtained from random tuning curves ($p < 0.001$; Wilcoxon rank sum test). Only 6% of the randomly generated tuning curves exhibited an $r^2 > 0.7$.

With regard to the influence of trial alignment on mEP tuning, we found that for most LFPs, the maximal SNR during the task was higher when the activity was aligned to movement onset (65 vs 35% of LFPs, the maximal SNR of which was higher when aligned to cue onset; SNR computed after smoothing with a Gaussian kernel of 125 ms standard width).

Using single mEPs and comparing the tuning curves belonging to two different peaks, we found that they were positively correlated if they belonged to peaks of equal sign and negatively correlated if the peaks were of a different sign (Fig. 3*a*). This structure in the mEP tuning became even more apparent if only the 56 LFPs with strongest tuning (best SNR during task >0.3; 13% of all LFPs) were considered. For these mEPs, the correlation of their tuning curves was −0.64 on average between peaks N1 and P2, −0.43 between N2 and P2, and 0.4 between N1 and N2 (all correlations were significant; $p < 0.001$; Wilcoxon rank sum test vs random tuning curves) (Fig. 3*a*). These correlations suggest that mEP tuning could reflect a simple directional modulation of the amplitude of a standardized complex waveform. We tested this model for LFP tuning in the following way: the time course of the smoothed LFP in trial i was modeled as $\mathrm{LFP}_i(t) = a_i \times \mathrm{mEP}(t) + c_i$, where a_i and c_i are the amplitude and offset in trial i, and $\mathrm{mEP}(t)$ is the LFP averaged across trials and directions. Figure 3*b* illustrates this model for the sample LFP: the best fit of the mEP (black) to a single trial for direction 5 (blue) was obtained by multiplying the mEP by a factor of 2.8. For different movement directions, the distributions of such amplitudes obtained differed (Fig. 3*c*), and LFPs could therefore be decoded on a single-trial basis (see Materials and Methods). The average decoding power that was achieved with this model for eight simultaneously recorded LFPs was 0.35, which was clearly better than chance level but significantly lower ($p < 0.001$; Wilcoxon signed rank test for paired samples) than the average decoding power of 0.47 achieved by decoding the full time course of the smoothed single-trial LFP activities from eight electrodes (see Materials and Methods for details). Hence, the amplitude modulation of the slow-complex LFP waveform contained a substantial amount but not all of the directional information of the smoothed LFP.

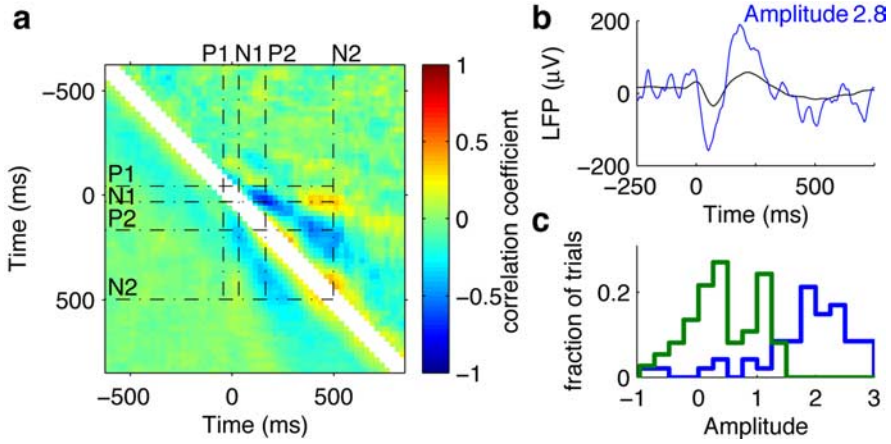

Figure 3. Simple model to decode LFP activity in the time domain. ***a***, Correlation between mEP tuning curves across time. Average correlation coefficient (color coded) between two tuning curves from the same LFP recording but at different time points, given by the *x* and *y* coordinates. The bottom left half of the matrix shows the mean across all 419 LFPs; the top right half represents the average across the 56 LFPs with strongest tuning (SNR > 0.3). ***b***, mEP of the sample LFP (Fig. 1*b*) averaged across all directions (black curve) and the LFP of a single trial (blue curve) during a movement to the left (180°) after low-pass filtering with a third-order Butterworth filter (cutoff frequency, 13 Hz). The mEP fitted the single trial activity best if multiplied by a scaling factor of 2.8 (see text for Materials and Methods as well as Results explanation). ***c***, Distributions of amplitudes (scaling factors) obtained for all single trials belonging to a movement to the right (0°, green histogram) and to the left (180°, blue histogram).

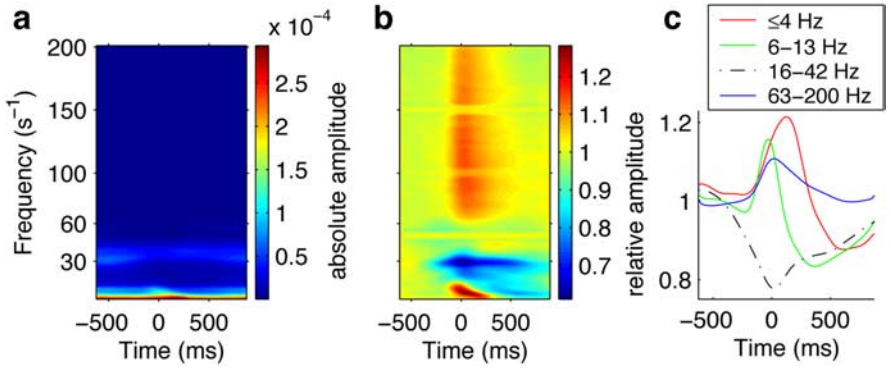

Figure 4. Characteristics of the LFP amplitude spectrum. Plots show averages across all electrodes and trials. ***a***, Time-resolved amplitude spectrum (arbitrary units). The 50 Hz noise was removed by applying a notch filter centered at 50 Hz. ***b***, Time-resolved amplitude spectrum as in ***a***, each frequency bin normalized by its baseline amplitude (see Materials and Methods). ***c***, Changes in amplitude exhibited by four different frequency bands (≤4, 6–13, 16–42, and 63–200 Hz) during the task.

LFP tuning in the frequency domain

The time-resolved amplitude spectrum, averaged across all electrodes, showed that the spectrum was dominated by frequencies <10 Hz and, to a lesser degree, by frequencies of ≈30 Hz (Fig. 4*a*). To detect movement-related changes in the amplitudes at different frequencies, we normalized the time-resolved amplitude of each frequency bin by its average amplitude during a baseline period before cue presentation (see Materials and Methods). This revealed that changes in amplitude occurred within several frequency ranges in the course of the trial (Fig. 4*b*). To further study the tuning in the frequency domain, we divided the frequency range into four bands (≤4, 6–13, 16–42, and 63–200 Hz), which exhibited homogeneous intraband temporal evolution of the normalized amplitude for many LFPs. Figure 4*c* shows the changes in normalized amplitude for these frequency bands during the task, averaged across all trials and electrodes. The amplitude of the 6–13 Hz band started to increase ≈100 ms before movement onset. During movement, this increase gradually became concentrated in lower frequencies (≤4 Hz), whereas the amplitude of the 6–13 Hz band declined. In contrast, the amplitude of the 16–42 Hz band substantially decreased around the time of the cue onset (≈250 ms before movement initiation) and remained below the amplitude of the baseline period during movement execution. The reduction of amplitude of this band was strongest around the time of movement onset. The increase in amplitude of the frequency band 63–200 Hz started around the same time as the increase in the low-frequency range (≤13 Hz) and lasted throughout the movement. The frequency range from 43 to 61 Hz was not investigated to avoid the power-line artifacts at ≈50 Hz.

How common is this behavior among the spectra of individual electrodes? The amplitude spectra of individual LFPs around movement onset were correlated with the normalized grand mean spectrum shown in Figure 4*b* with a median correlation of 0.59. With regard to the changes in the individual frequency bands depicted in Figure 4*c*, 244 of 419 (58%) of all LFP spectra showed a significant increase ($p < 0.05$; see Materials and Methods) in the ≤4 Hz band, 254 of 419 (61%) showed a significant increase in the 6–13 Hz band, 358 of 419 (85%) showed a significant decrease in the 16–42 Hz band, and 287 of 419 (69%) showed a significant increase in the 63–200 Hz band. Nearly one-third (124 of 419; 30%) of all electrode spectra followed the general behavior depicted in Figure 4*c* for all four frequency bands (i.e., a significant increase in amplitudes during movement in the ≤4, 6–13, and 63–200 Hz bands and a significant decrease in amplitudes during movement in the 16–42 Hz band).

Next, we investigated how the amplitude modulation in these frequency bands depended on movement direction. Figure 5*a* shows the temporal evolution of the normalized amplitude spectrum separately for each movement direction for the sample LFP (same as in Figs. 1*b–d*, 2*a*). Evidently, for this LFP, both the amplitudes of low frequencies (≤13 Hz) and high frequencies (63–200 Hz) varied with the direction of movement. Figure 5*b* depicts the tuning curves obtained for the ≤4, 6–13, and 63–200 Hz frequency bands at the time where their respective signal-to-noise ratio was highest (160, 40, and 20 ms after movement onset, respectively) (see Fig. 5*c* for the temporal evolution of SNR). Each tuning curve fitted a cosine function very well ($r^2 = 0.87$, 0.95, and 0.91 for the ≤4, 6–13, and 63–200 Hz bands, respectively). Interestingly, while all three bands were directionally tuned, their PDs differed significantly ($p < 0.001$; Wilcoxon rank sum test of bootstrap distribution of PDs): the PD shifted from 200° for the ≤4 Hz band, via 182° for the 6–13 Hz band, to 153° for the 63–200 Hz band (Fig. 5*b*, right). The time-resolved SNR (Fig. 5*c*) of both the 6–13 and 63–200 Hz bands increased before movement onset and were clearly >0 until 200 ms after movement initiation. The SNR of the ≤4 Hz band exhibited a strong increase after movement onset, which lasted longer than the increases in

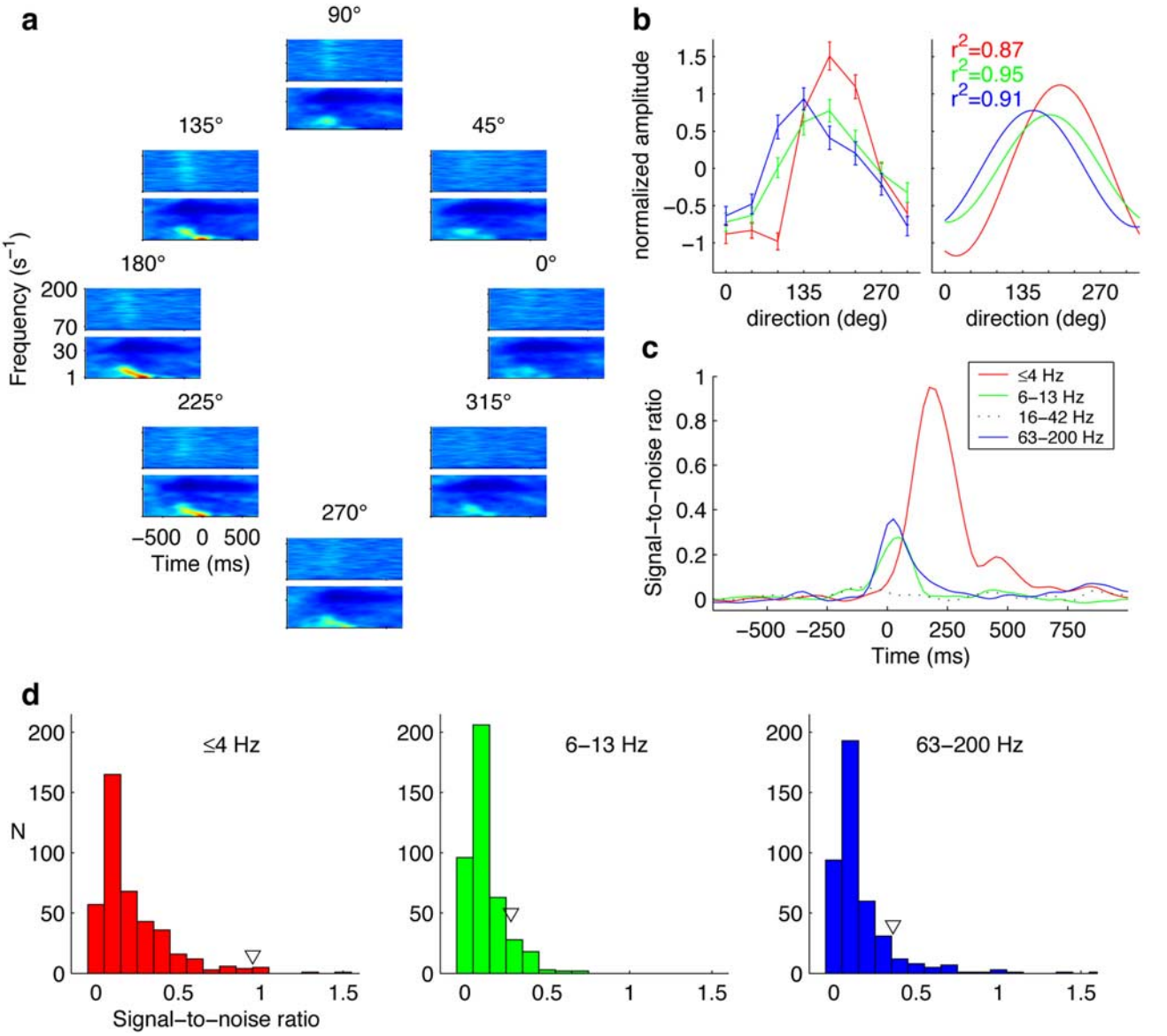

Figure 5. LFP tuning in the frequency domain. ***a***, Time-resolved and normalized amplitude spectrum obtained from one sample electrode (same as in Fig. 1*b–d*), separately for each movement direction. ***b***, Left, Normalized tuning curves (including SEMs) of the LFP amplitude spectrum shown in ***a*** for three different frequency bands (≤4, 6–13, and 63–200 Hz). Tuning curves were normalized by subtracting the mean and dividing by the SD across trials averaged across eight directions. Each tuning curve was computed at the time point in which the signal-to-noise ratio of the respective frequency band was highest (compare ***c***). Right, Cosine functions fitted to the curves on the left. Numbers show the squared correlation coefficients between data and the fitted cosine function. ***c***, Signal-to-noise ratios of the LFP amplitude spectrum shown in ***a***, separately for the different frequency bands. Time is relative to movement onset. ***d***, Distributions of SNRs across all LFPs for the ≤4, 6–13, and 63–200 Hz bands. For each LFP and frequency band, the best SNR between 200 ms before movement onset and 750 ms after movement onset was chosen. The triangle denotes the SNR values of the sample LFP.

the 6–13 and 63–200 Hz bands. In contrast, the 16–42 Hz band showed no increase in its SNR throughout the task (Fig. 5*c*).

Comparison of the SNRs of the ≤4, 6–13, and 63–200 Hz bands across all LFPs revealed a skewed distribution for each band, centered on SNRs between 0 and 0.3, with few higher values in the right tail of the distribution (Fig. 5*d*). We compared the time-resolved SNRs of the different frequency bands averaged across all LFPs and separately for movements of the contralateral and ipsilateral arm (Fig. 6*a*). The maximal SNR of the ≤4 Hz band occurred 200 ms after movement onset and was nearly of equal strength for both contralateral and ipsilateral movements (0.13 and 0.11, respectively). The maximal SNRs of the 6–13 and 63–200 Hz bands occurred around movement onset and were clearly higher during contralateral than during ipsilateral movements (0.09 vs 0.05 and 0.14 vs 0.04, respectively). In contrast, the average SNR of the 16–42 Hz band did not exceed 0.03.

We also analyzed the data for cosine tuning curves in the frequency domain. As in the time domain, LFPs with significant tuning frequently showed high-correlation values for cosine tuning during the task. For example, a fit with $r^2 > 0.7$ was found for the frequency band ≤4 Hz at P2 in 38% of the significantly tuned LFPs, for the frequency band 6–13 Hz at N1 in 27%, and for the frequency band 63–200 Hz at peak P1 in 56% (Fig. 6*b*). The medians of the r^2 distributions were significantly higher ($p < 0.001$; Wilcoxon rank sum test during all four peaks and for all three frequency bands, except for 6–13 Hz at P1) than expected for random tuning curves, where only 6% had an r^2 value >0.7. The distributions of the corresponding PDs of each frequency

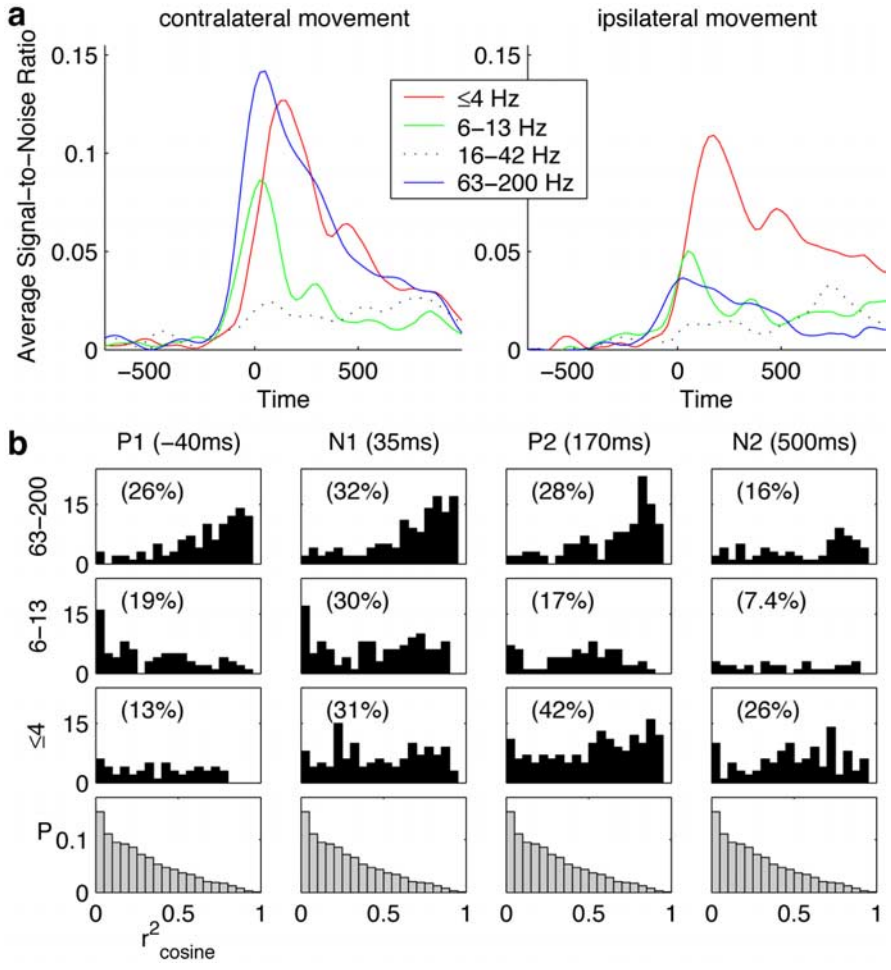

Figure 6. Tuning properties of LFPs in the frequency domain. ***a***, Average tuning strength of different LFP frequency bands. Each curve depicts the time-resolved (movement onset at $t = 0$ ms) signal-to-noise ratio of a certain frequency band (see inset), averaged across all recorded LFPs, separately for contralateral (left) and ipsilateral (right) movements. ***b***, Correlation between tuning curves derived from LFP amplitude spectra and best cosine fit. Only LFPs with significant tuning ($p < 0.05$; see Materials and Methods) in the corresponding frequency band at the selected time point were considered; their percentage is given in parentheses. Black histograms show the distribution of r^2 values across these LFPs at P1, N1, P2, and N2 (columns, times following P1, N1, P2, and N2 denote the time relative to movement onset) and for three different frequency bands (rows). Gray histograms (bottom) show the probability distribution of r^2 values obtained for random tuning curves (see Materials and Methods).

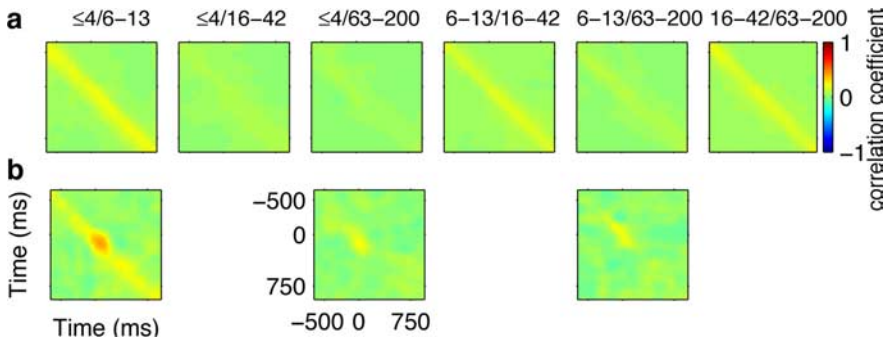

Figure 7. Signal and noise correlation between two different frequency bands. Time 0 ms indicates movement onset. ***a***, Noise correlations. Correlation between trial-by-trial fluctuations of two different frequency bands (indicated on top) for all combinations of time delay between the two bands is shown. *x* and *y* coordinates indicate the time point of measurement for the second and the first frequency bands, respectively. Data were averaged across all recorded LFPs. ***b***, Signal correlation. Correlation between the tuning curves of two different frequency bands (indicated at the top) for all combinations of time delay between the two bands is shown. *x* and *y* coordinates indicate the time point of measurement of tuning curves for the second and the first frequency bands, respectively. Data were averaged across all recorded LFPs, with significant tuning ($p < 0.01$) occurring in both bands during the course of the task.

band exhibited no or only weak deviation from a uniform distribution between 0 and 360° ($p = 0.37$, 0.03, and 0.10; Kolmogorov–Smirnov test) for the ≤4, 6–13, and 63–200 Hz bands, respectively (only LFPs with significant tuning and r^2 for cosine tuning >0.7 were taken into account).

To determine the extent to which the neuronal activities in different frequency bands were independent of each other, we calculated the signal and noise correlations between pairs of different frequency bands in the same LFP (see Materials and Methods). The signal correlation measures the similarity of the tuning curves, whereas the noise correlation measures the correlation of the trial-by-trial fluctuations. Generally, the noise correlations between frequency bands were weak (Fig. 7*a*), fluctuations in the amplitude of one band occurred mostly independently of fluctuations in another band of the same LFP. For zero time delay between the activities of the two bands, the noise correlations were weakly positive on average: ≈0.2 between neighboring bands (≤4 and 6–13 Hz, 6–13 and 16–42 Hz, and 16–42 and 63–200 Hz) and ≈0.1 between non-neighboring bands (≤4 and 16–42 Hz, ≤4 and 63–200 Hz, and 6–13 and 63–200 Hz). For a time delay different from 0, the noise correlation was ≈0 on average for all pairs (Fig. 7*a*). To investigate the signal correlations between different frequency bands, only LFPs with significant tuning ($p < 0.01$) during the task for both respective bands were selected (154, 156, and 114 of 419 LFPs for the ≤4 vs 6–13 Hz bands, the ≤4 vs 63–200 Hz bands, and the 6–13 vs 63–200 Hz bands, respectively). We found that tuning curves from two different frequency bands were similar only to a small degree: tuning curves from the ≤4 and 6–13 Hz bands were slightly stronger correlated (maximum, 0.45) than the tuning curves from the ≤4 and 63–200 Hz bands or the 6–13 and 63–200 Hz bands (maxima, 0.22 and 0.24) (Fig. 7*b*).

Decoding of movement direction from single-trial LFP amplitude spectra

The LFP frequency bands that were tuned to movement direction were further analyzed to explore their DP, a measure to quantify how well one can infer the movement direction on a single-trial basis, now using the LFP amplitude spectra. To this end, we used regularized linear discriminant analysis for classification and computed the decoding power as the number of correctly classified trials divided by the total number of decoded trials (see Materials and Methods for additional details).

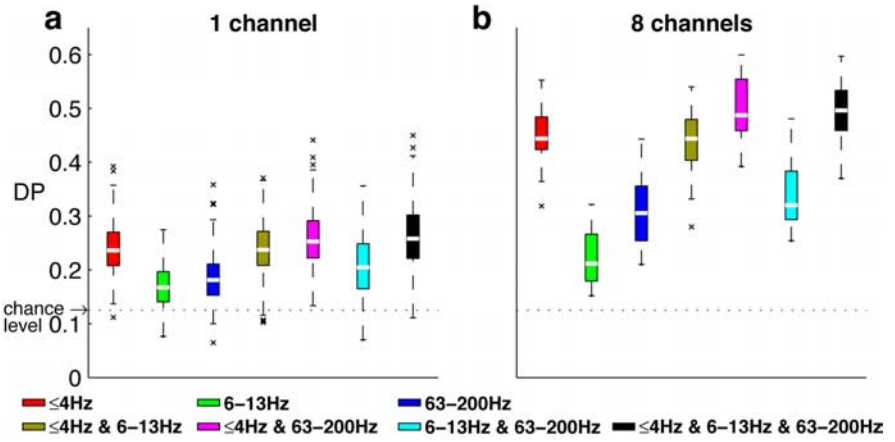

Figure 8. Decoding power of different frequency bands. ***a***, The box plots show the distribution of decoding power of single LFPs for various frequency bands and their combinations indicated at the bottom. White bars depict the median, the box ranges from the lower to the upper quartiles, the dashed whiskers extend to the most extreme decoding power within the 1.5-fold interquartile range from the borders of the bars, and the × symbols mark outliers. ***b***, Decoding power of simultaneous LFP recordings from eight electrodes (symbols as in ***a***).

Figure 8 shows the distributions of decoding power for the three frequency bands and their combinations (color coded), computed for signals from single electrodes (Fig. 8*a*) and for signals from eight simultaneously recorded electrodes (Fig. 8*b*). To estimate the decoding power for a larger multielectrode array with electrode spacing comparable with ours, we additionally computed the decoding power for 48 LFP channels (from data recorded in six separate sessions with eight channels per session). Qualitatively, for these three computations, our results were similar: with an increasing number of electrodes [from 1 to 8 (compare Fig. 8) and from 8 to 48], the decoding power increased for all three frequency bands and their various combinations. Regardless of the number of electrodes, the low-frequency band (≤4 Hz) yielded the best decoding power (median DP of 0.24, 0.44, and 0.83 for 1 electrode, 8 electrodes recorded simultaneously, and 48 electrode estimate, respectively), followed by the high-frequency band (63–200 Hz; 0.18, 0.31, and 0.63 respectively), and the intermediate band (6–13 Hz; 0.17, 0.21, and 0.39, respectively). Figure 8 also shows that combining two frequency bands can increase the decoding power: the highest DP was achieved by the combination of the ≤4 and 63–200 Hz frequency bands (median DP of 0.25, 0.49, and 0.88 for 1 electrode, 8 simultaneously recorded electrodes, and the estimated 48 electrode case, respectively), the remaining combinations including the intermediate frequency band (6–13 Hz) clearly carried less information about movement direction.

The combination of all three frequency bands (median DP of 0.26, 0.50, and 0.86 for 1 electrode, 8 simultaneously recorded electrodes, and the estimated 48 electrode case, respectively) did not further increase the DP. This is because of the fact that the relatively low amount of additional information added by the intermediate frequency band competes with the decrease in performance of the decoder as a result of the higher number of input signals.

Concerning the estimate of decoding power for 48 LFP channels, however, we point out that, depending on the signal and noise correlations between channels, the actual decoding power in a true 48-channel recording could differ substantially from the estimates presented here (cf. Abbott and Dayan, 1999; Schneidman et al., 2003).

Discussion

This study reveals distinct features of local field potentials in the motor cortex during the performance of arm movements. Using additional data from the experiments described in a previous study (Mehring et al., 2003), we describe new LFP tuning properties in the time domain. Moreover, we show that LFP tuning is manifested also, and differentially, in oscillatory activities in different frequency ranges (≤4, 6–13, and 63–200 Hz). In both the time and frequency domains, a cosine function could describe the tuning well.

Although the experiment was not designed to distinguish between neuronal tuning to direction of movement and tuning to direction or location of the target, the fact that the best tuning in individual LFPs was obtained by alignment to movement onset in most LFPs but also by alignment to cue signal for approximately one-third of the LFPs, hints at a more complex involvement of LFPs in the control of voluntary movements [for tuning without movement, see Georgopoulos et al. (1989); for motor cortical responses to visual stimuli, see Merchant et al. (2001)].

Relationship between low-frequency oscillations (≤13 Hz) and movements

Our results show that the amplitude of lower frequencies (≤13 Hz) is modulated with the direction of movement. The directional tuning of the frequency band 6–13 Hz precedes the directional tuning of the lowest frequency band (≤4 Hz). This is in good agreement with the tuning of the amplitude of the mEP, found by analyzing the LFP in the time domain: the mEP oscillates between several positive and negative peaks, and the oscillation slows down from movement onset toward movement end.

Relationship between high-frequency oscillations (16–200 Hz) and movements

Fast oscillations of motor cortical LFP activity have been investigated previously in a number of studies in monkeys (Murthy and Fetz, 1992; Sanes and Donoghue, 1993; Donoghue et al., 1998; Baker et al., 1999). Likewise, the relationship between movements and fast oscillations of the ECoG and EEG has been investigated in humans (Crone et al., 1998; Aoki et al., 1999; Pfurtscheller et al., 2003; Leuthardt et al., 2004). Studies conducted in monkeys attempted to relate oscillations between 15 and 50 Hz to different aspects of behavior. For example, 25–35 Hz oscillations were reported to occur during exploratory behavior (Murthy and Fetz, 1992), 15–50 Hz oscillations were found to increase in relation to movement preparation and decrease during movement execution (Donoghue et al., 1998), and 20–30 Hz oscillatory activity of LFPs was reported to occur increasingly during maintenance of a precise grip (Baker et al., 1999). Studies conducted in humans reported that high-frequency (30–90 Hz) amplitudes often increased during movements, whereas the amplitude of oscillations between 15 and 30 Hz decreased (Aoki et al., 1999; Pfurtscheller et al., 2003). Leuthardt et al. (2004) observed a direction-dependent increase in amplitudes in the high-frequency (40–180 Hz) band of human ECoG recordings during joystick movements in four different directions.

In our recordings, we found a clear difference in the behavior of the 16–42 and 63–200 Hz bands: the amplitude of the 16–42 Hz band decreased during movement execution, confirming previous results for monkeys and humans (Sanes et al., 1993; Donoghue et al., 1998; Pfurtscheller et al., 2003). Furthermore, in our study, the 16–42 Hz band was not tuned to the direction of movement. In contrast, the amplitude of the 63–200 Hz band increased during movement. An increase in high-gamma band activity around movement onset was also reported in ECoG studies on humans [shown for 75–100 Hz by Crone et al. (1998) and for 60–90 Hz by Pfurtscheller et al. (2003)]. Interestingly, in our recordings, we found that the amplitude of the frequency band from 63–200 Hz was additionally modulated by the direction of movement. We conclude that the intermediate frequency range may have a different functional role in motor control than high-frequency (63–200 Hz) and low-frequency (≤13 Hz) ranges.

Even if some aspects of spiking activity might be reflected in the 63–200 Hz frequency band, they could not be explained by the spiking activity of nearby neurons (see Materials and Methods for details). Thus, we also conclude that the 63–200 Hz frequency band reflects, at least to a large degree, a supplementary signal not contained in the superimposed spike trains (MUA).

Functional meaning of high-frequency oscillations

To elucidate the functional implications of our results concerning high-frequency (16–200 Hz) oscillations, we considered the following four hypotheses. First, high-frequency oscillations are merely a consequence of increased cortical excitability (Aoki et al., 1999). Second, high-frequency oscillations are a signature of combining ("binding") movement primitives (considered as being represented by neuronal assemblies) into a complex movement (for a similar notion in visual processing, see Singer, 1993; Singer and Gray, 1995). The combining could occur either during execution or during preparation of movement (Murthy and Fetz, 1992; Donoghue et al., 1998). Third, high-frequency oscillatory activity reflects different levels of attention (Murthy and Fetz, 1992; Fries et al., 2002). Fourth, in contrast, results from other studies would be compatible with a hypothesis in which high-frequency oscillations reflect cortical computation of details of movement execution (Baker et al., 1999; Feige et al., 2000).

Most importantly, our results clearly show that activity in an ≈30 Hz band (i.e., 16–42 Hz) and frequency components higher than 62 Hz behave in distinctly different ways. The cosine-like directional modulation of the high-frequency amplitudes we found in the 63–200 Hz band indicates that this type of activity could indeed be related to details of movement execution, similar to the firing rate of single neurons.

The increase in amplitude of frequencies >60 Hz around movement onset supports the first, second, and fourth hypotheses, because neuronal excitability and mechanisms of motor binding and computation should be enhanced at movement onset and during movement execution. In contrast, this increase argues against the third hypothesis, because the level of attention should be relatively high around the time of cue presentation and low(er) during the execution of a stereotyped movement. Note that the movement-related increase in the 63–200 Hz band was also evident when the LFPs were aligned to the time of cue onset (data not shown): the amplitude of the 63–200 Hz band was lowest before cue presentation and started to increase only after cue presentation.

Activity in the ≈30 Hz band, however, was not modulated with the direction of arm movement. This behavior is in agreement with a hypothesis of a more global and less specific involvement in the task, conforming to the first and third hypotheses. For the ≈30 Hz band, the amplitude was highest before the presentation of the cue signal and lowest around movement onset, which also supports the third hypothesis, because attention should be high in expectance of a movement stimulus and low during the execution of a stereotyped movement. Again, aligning the LFPs to the time of cue onset confirmed these findings.

Thus, oscillations from 63–200 Hz could reflect both global aspects (like the combining of different movement primitives) and the computation of specific movement parameters (second and fourth hypotheses). Oscillations of ≈30 Hz, in contrast, could reflect the level of excitability or attention (first and third hypotheses). Additional studies are required to further differentiate between any of these possibilities for each respective frequency range.

Relevance for brain computer interfaces

Our results show that motor cortical LFPs have some remarkable similarities to motor cortical single-unit activity. Both LFPs and SUA have a strong tendency for cosine-like directional tuning and can be used for the decoding of movement direction. Combining these findings with previous results, which demonstrated that LFPs carry substantial information about a planned and/or executed movement (Pesaran et al., 2002; Mehring et al., 2003), the use of LFPs as an alternative (or additional) neuronal control signal for brain–machine interfaces based on intracranially implanted electrodes is suggested. This is of great interest for such applications, because the recording of LFPs is simpler and expected to have a better long-term stability than the recording of SUA. Moreover, the decoding of LFPs can be performed directly on the raw signals, as opposed to the decoding of single-unit activity in which previous spike sorting (cf. Wood et al., 2004) is inevitable.

Furthermore, because the sources of the LFP are assumed to be essentially the same as those for the ECoG and the EEG (Mitzdorf, 1985; Creutzfeld, 1995), our results suggest that the features of the LFP that are relevant for the inference of arm movements could also be the basis for movement decoding from ECoG and EEG signals. Recently, it has been shown that the direction of purposeful arm movements can be inferred from neuronal population activity measured with electrodes placed directly on the surface of the human frontal cortex (Leuthardt et al., 2004; Mehring et al., 2005). In these studies, both low- and high-frequency components were shown to carry information about arm movements. In contrast, no study on the EEG thus far used frequencies >60 Hz to decode information about arm movements. Thus, investigations of the high-frequency components of human ECoG and also EEG signals, in a similar manner as presented here for LFPs, may improve future brain–machine interfaces based on these signals.

References

Abbott LF, Dayan P (1999) The effect of correlated variability on the accuracy of a population code. Neural Comput 11:91–101.

Andersen R, Musallam S, Pesaran B (2004) Selecting the signals for a brain-machine interface. Curr Opin Neurobiol 14:720–726.

Aoki F, Fetz EE, Shupe L, Lettich E, Ojemanm A (1999) Increased gamma-range activity in human sensorimotor cortex during performance of visuomotor tasks. Clin Neurophys 110:524–537.

Baker SN, Kilner JM, Pinches EM, Lemon RN (1999) The role of synchrony and oscillations in the motor output. Exp Brain Res 128:109–117.

Carmena JM, Lebedev MA, Crist RE, O'Doherty JE, Santucci DM, Dimitrov D, Patil PG, Henriquez CS, Nicolelis MA (2003) Learning to control a brain-machine interface for reaching and grasping by primates. PLoS Biol 1:E42.

Creutzfeld OD (1995) Cortex cerebri: performance, structural and functional organization of the cortex, Chap 5. Oxford: Oxford UP.

Crone NE, Miglioretti DL, Gordon B, Lesser RP (1998) Functional mapping of human sensorimotor cortex with electrocorticographic spectral analysis. Brain 121:2301–2315.

Donchin O, Gribova A, Steinberg O, Bergman H, Cardoso de Oliveira S, Vaadia E (2001) Local field potentials related to bimanual movements in the primary and supplementary motor cortices. Exp Brain Res 140:46–55.

Donoghue JP, Sanes JM, Hatsopoulos NG, Gaal G (1998) Neural discharge and local field potentials oscillations in primate motor cortex during voluntary movements. J Neurophysiol 79:159–173.

Feige B, Aertsen A, Kristeva-Feige R (2000) Dynamic synchronization between multiple cortical motor areas and muscle activity in phasic voluntary movements. J Neurophysiol 84:2622–2629.

Friedman JH (1989) Regularized discriminant analysis. J Am Stat Assoc 84:165–175.

Fries P, Schroeder J-H, Roelfsema PR, Singer W, Engel AK (2002) Oscillatory neuronal synchronization in primary visual cortex as a correlate of stimulus selection. J Neurosci 22:3739–3754.

Georgopoulos AP, Crutcher MD, Schwartz AB (1989) Cognitive spatial-motor processes. III. Motor cortical prediction of movement direction during an instructed delay period. Exp Brain Res 75:183–194.

Leuthardt EC, Schalk G, Wolpaw JR, Ojemann JG, Moran, DW (2004) A brain-computer interface using electrocorticographic signals in humans. J Neural Eng 1:63–71.

Mehring C, Rickert J, Vaadia E, Cardoso de Oliveira S, Aertsen A, Rotter S (2003) Inference of hand movements from local field potentials in monkey motor cortex. Nat Neurosci 6:1253–1254.

Mehring C, Nawrot MP, Cardoso de Oliveira S, Vaadia E, Schulze-Bonhage A, Aertsen A, Ball T (2005) Comparing information about arm movement direction in single channels of local and epicortical field potentials from monkey and human motor cortex. J Physiol (Paris), in press.

Merchant H, Battaglia-Mayer A, Georgopoulos AP (2001) Effects of optic flow in motor cortex and area 7a. J Neurophysiol 86:1937–1954.

Mitzdorf U (1985) Current source-density method and application in cat cerebral cortex: investigation of evoked potentials and EEG phenomena. Physiol Rev 65:37–100.

Murthy VN, Fetz EE (1992) Coherent 25- to 35-Hz oscillations in the sensorimotor cortex of awake behaving monkeys. Proc Natl Acad Sci USA 89:5670–5674.

Pesaran B, Pezaris JS, Sahani M, Mitra PP, Andersen RA (2002) Temporal structure in neuronal activity during working memory in macaque parietal cortex. Nat Neurosci 5:805–811.

Pfurtscheller G, Graimann B, Huggins JE, Levine SP, Schuh LA (2003) Spatiotemporal patterns of beta desynchronization and gamma synchronization in corticographic data during self-paced movement. Clin Neurophys 114:1226–1236.

Press WH, Flannery BP, Teukolsky SA, Vetterling TW (1992) Numerical recipes in C: the art of scientific computing, Chap 12, 13. Cambridge, UK Cambridge UP.

Sanes JN, Donoghue JP (1993) Oscillations in local field potentials of the primate motor cortex during voluntary movement. Proc Natl Acad Sci USA 90:4470–4474.

Schneidman E, Bialek W, Berry Jr MJ (2003) Synergy, redundancy, and independence in population codes. J Neurosci 23:11539–11553.

Serruya MD, Hatsopoulos NG, Paninski L, Fellows MR, Donoghue JP (2002) Instant neural control of a movement signal. Nature 416:141–142.

Singer W (1993) Neuronal representations, assemblies and temporal coherence. Prog Brain Res 95:461–474.

Singer W, Gray CM (1995) Visual feature integration and the temporal correlation hypothesis. Annu Rev Neurosci 18:555–586.

Smith JO (2003) Mathematics of the discrete Fourier transformation (DFT), with music and audio applications. W3K Publishing. E-book available at http://ccrma.stanford.edu/~jos/mdft.

Taylor DM, Tillery SI, Schwartz AB (2002) Direct cortical control of 3D neuroprosthetic devices. Science 296:1829–1832.

Wolpaw JR, Birbaumer N, McFarland DJ, Pfurtscheller G, Vaughan TM (2002) Brain-computer interfaces for communication and control. Clin Neurophysiol 113:767–791.

Wolpaw JR, McFarland DJ (2004) Control of a two-dimensional movement signal by a noninvasive brain-computer interface in humans. Proc Natl Acad Sci USA 101:17849–17854.

Wood F, Black MJ, Vargas-Irwin C, Fellows M, Donoghue JP (2004) On the variability of manual spike sorting. IEEE Trans Biomed Eng 51:912–918.